CYCLIC CONSOLIDATION AND AXIAL FRICTION FOR SEABED PIPELINES

Y. Yan[1], D. J. White[1] and M. F. Randolph[1]

Keywords: Offshore engineering, Pipelines, Consolidation, Numerical modelling

ABSTRACT

This paper presents finite element analyses of the axial sliding resistance of a seabed pipeline embedded in soft normally consolidated Modified Cam clay. The study demonstrates the rise in axial resistance associated with episodes of movement with intervening periods of consolidation. It is shown that the excess pore pressures generated during undrained axial movements lead to significant consolidation and strength gain in the surrounding soil.

For Modified Cam clay, using properties representative of kaolin, the resistance rises exponentially with cycles and reaches the drained limit within approximately 10-20 episodes of movement and consolidation. The rate of gain in resistance is shown to be controlled by the volumetric stiffness ratio, κ/λ, for soil that is initially normally consolidated.

Simple relationships are proposed that will assist in utilizing this beneficial phenomenon in design practice. The increase in axial sliding resistance due to consolidation may mean that mitigation requirements against cyclic axial pipe walking, caused by thermal expansion, may be reduced or eliminated.

Words: 1978

Figures: 7

Tables: 2

[1] *Centre for Offshore Foundation Systems, The University of Western Australia, Crawley, WA 6009, Australia (Corresponding author: David White, david.white@uwa.edu.au)*

INTRODUCTION

Pipe 'walking' is the unwanted accumulation of axial movement of a seabed pipeline during cycles of operation. This is an increasingly significant design challenge as operating pressures and temperatures rise for pipelines on soft fine-grained soils. The rate at which a pipeline will axially 'walk' during cycles of startup and shutdown is strongly influenced by the axial pipe-soil sliding resistance.

The first comprehensive study of pipe walking was reported by Tornes et al (2000) and analytical solutions linking pipe-soil friction and pipe walking rate for simple scenarios were published by Carr et al. (2006). A significant quantity of experimental data on axial pipe-soil resistance was collated by White et al. (2011), showing the influence of drainage and excess pore pressure. White & Cathie (2011) set out a framework for axial pipe-soil resistance based on an effective stress approach, spanning both undrained and drained conditions. It was proposed that the axial resistance during cycles of pipeline movement will tend towards the drained value, regardless of the rate or duration of each movement event, because the soil surrounding the pipe will eventually consolidate to a critical state at which excess pore pressure generation will not occur. There is a significant design benefit if this mechanism can be reliably predicted, since the drained resistance is typically higher than the undrained resistance. A narrower and higher design range of axial friction leads to less onerous walking mitigation measures such as reduced anchoring requirements.

To capture this mechanism a quantitative analytical framework based on planar shearing with concurrent drainage and consolidation was introduced by Randolph et al. (2012), using critical state theory. This solution describes the transition from undrained to drained axial pipe-soil resistance due to consolidation concurrent with pipe movement. The results were validated for the curved geometry of a pipeline by finite element analyses of axial pipe-seabed interaction with coupled consolidation, and these results are described further by Yan (2014).

This paper extends the previous work to the situation in which consolidation occurs between pipe movement events, which are themselves undrained. This situation represents typical pipeline operating behaviour on soft marine clays. The pipe moves axially during the process of starting up or shutting down the pipeline. During the intervening period when the pipe is either in operation or is shut down, any excess pore pressure in the surrounding soil dissipates, causing a change in strength and therefore sliding resistance during the subsequent axial movement.

FINITE-ELEMENT METHODOLOGY

Three dimensional coupled small strain finite element analyses have been undertaken using the Modified Cam clay soil model (Roscoe and Burland 1968), as implemented in ABAQUS.

An infinite length of pipe was modelled by a narrow prism of elements, constrained so the nodes on the vertical planes confining the prism moved identically, as described by Randolph et al. (2012). The pipe was modelled as a 0.5 m diameter rigid circular body with a fully rough surface, pre-embedded to a depth of 0.3 diameters. The embedded pipe nodes were tied to the adjacent soil elements.

The soil was defined as a linear elastic - plastic material. All parameters adopted in the numerical analyses are listed in Table 1. The soil body was initially consolidated with K_0 = 0.6 and an artificial 0.001 kPa surcharge on the top surface to provide computational stability. These initial conditions cause the strength and other properties (in particular the initial c_v, and e) to vary with depth, following standard relationships (Wroth 1984). A fine mesh was assigned close to the pipe, reducing to an element size of 0.002D at the pipe-soil interface to eliminate mesh density effects. Further details of the adopted Modified Cam clay soil model and FE modelling methods used in the present study are described by Randolph et al. (2012), Chatterjee et al. (2012) and Yan (2014). Dimensionless values of time, $T = c_{v0}t/D^2$ and velocity, $V = vD/c_{v0}$, were assessed using the initial c_{v0} value at the depth of the pipe invert (0.15 m). This value is derived using the initial soil state and plastic isotropic compressibility ($m_v = \lambda/(1+e_0)/p'_0$) and is shown in Table 1.

ANALYSIS PROCEDURES

The analyses involved firstly applying a simulated weight of the pipeline equal to the ultimate vertical bearing capacity (V/D~1.7 kPa) at the adopted pipe invert embedment of 0.3 diameters. This vertical load was applied for a period sufficient for full dissipation of the excess pore pressure created by the pipe weight, and then was maintained constant for the remainder of the analysis.

The pipe was then subjected to different sliding episodes:

1. *Single sliding events – undrained and drained at failure.* The pipe was subjected to continuous axial movement with constant velocities of vD/c_{v0} = 2000 (undrained failure) and 0.2 (drained failure) for sufficient sliding distance to identify the fully drained resistance. These two cases have been reported previously (Randolph et al.

2012, Yan 2014). The undrained failure case forms the fundamental 'backbone' curve for concurrent sliding and consolidation in which failure is reached prior to any significant pore pressure dissipation. After failure, the resistance rises progressively from the undrained limit to the drained limit. In the drained case the dissipation occurs more rapidly than the mobilization of the sliding resistance, which only reaches a plateau at the drained limit.

2. *Cyclic sliding event – undrained at failure.* The pipe was subjected to a series of undrained sliding events, with intervening periods of full excess pore pressure dissipation, to represent typical operational conditions. The movements were at a velocity of vD/c_{v0} = 2000 over a sufficient distance for the undrained resistance to be fully mobilized, without significant excess pore pressure dissipation. 20 cycles of movement and consolidation were simulated. The base case cyclic sliding analysis used the parameters given in Table 1, and two additional cases used alternative values of λ and κ, as discussed later.

RESULTS

Sliding resistance and pore pressure dissipation

The base case cyclic sliding analysis showed an increase in axial pipe-soil resistance consistent with the cyclic hardening mechanism proposed by White & Cathie (2011). The equivalent axial friction factor during the initial movement is 0.32, which is consistent with the normally consolidated strength ratio of the soil, enhanced slightly by wedging around the pipe periphery (White & Randolph 2007). After 20 cycles, the resistance has risen close to the drained limit given by an interface friction of tan ϕ (Figure 1), which is consistent with model test observations (Smith & White 2014).

The changes in excess pore pressure are described by the normalized quantity, $r_u = (\Delta u_{av}/\sigma_{Nav})$ where Δu_{av} is the excess pore pressure and σ_{Nav} is the normal pipe-soil stress, averaged around the pipe-soil interface. The rise and fall in r_u with each episode of sliding and reconsolidation is shown in Figure 2, with the dimensionless time reset at the start of each movement. Higher excess pore pressure is generated in the early sweeps, consistent with the lower sliding resistance. The normalised dissipation response is fitted approximately by the relationship:

$$\frac{\Delta u_{av}}{\Delta u_{av,i}} = \frac{1}{1+(T/T_{50})^m} \quad (1)$$

where T_{50} is the value of T for 50% dissipation and m is a constant (see Figure 3 and Table 2).T_{50} decreases during the first few episodes, and remains stable at $T_{50} \sim 0.004$ from sweep 8 onwards. Consolidation is practically complete by $T \sim 0.3$.

The intermittent sliding case is compared to the monotonic fast and slow sliding cases in Figure 4, without 'resetting' the time axis to zero at the start of each intermittent sweep. The fast monotonic sliding case shows the undrained-drained backbone response for continuous shearing, as analysed previously by Randolph et al. (2012). This response provides benchmark values of the fully undrained and fully drained sliding resistance, with the latter value being reached at a dimensionless time of $T \sim 1$. The slow monotonic case confirms the drained sliding resistance, and reaches this value slightly later. The intermittent cyclic sliding case reaches the same drained resistance limit, but after a cumulative time of $T \sim 5$, and 20 pipe movement events totalling only $T \sim 10^{-4}$ in duration.

To predict the rate of hardening for intermittent cyclic sliding it is clearly necessary to instead consider the accumulated cycles of shearing and dissipation rather than the cumulative movement time or the overall elapsed time.

Cyclic evolution of sliding resistance

The measured variation in sliding resistance is shown in Figure 5 in a normalised manner as the drainage index, Ψ, which varies from 0 to 1 as the current resistance, (F/W), rises from the initial undrained limit, $(F/W)_{undrained}$, to the drained limit, $(F/W)_{drained}$:

$$\Psi = \frac{\frac{F}{W} - \left(\frac{F}{W}\right)_{undrained}}{\left(\frac{F}{W}\right)_{drained} - \left(\frac{F}{W}\right)_{undrained}} \quad (2)$$

The resistance mobilised during the n^{th} sweep can be fitted by a simple power law:

$$\Psi = 1 - \exp^{-0.7(n-1)/N_{50}} \quad (3)$$

The parameter N_{50} is the number of cycles of movement and consolidation required to achieve 50% of the full hardening process, or a drainage index of $\Psi = 0.5$. As shown by the stress paths discussed below, the hardening effect depends on the reduction in moisture content. The final reduction in moisture content depends on the steepness of the critical state line, λ, whilst the reduction during each reconsolidation event depends on the unload-reload gradient, κ. There is therefore a dependency of N_{50} on the ratio κ/λ (or alternatively the volumetric strain ratio, $\Lambda = 1 - \kappa/\lambda$), which is illustrated by the results from two additional

cyclic analysis cases shown on Figure 5. By doubling κ or by halving λ, the rate of hardening is doubled.

A simple relationship to capture this effect is:

$$N_{50} = \frac{0.9}{\kappa/\lambda} \quad (4)$$

which leads to the two fitted curves shown in Figure 5 that show good agreement with the numerical results.

Equations 3 and 4 require extending to cover cases in which the soil is initially over-consolidated and the cyclic hardening rate will depend on other aspects of the soil model, such as the spacing ratio between the normal compression and critical state lines. The ratio κ/λ alone is unlikely to capture all aspects of the cyclic hardening in natural soils, particularly when there is significant structure.

Stress paths beneath pipe invert

The effective stress and stress:volume paths followed by a soil element located immediately beneath the pipe invert are shown in Figure 6. During initial loading of the pipe the effective stress reduces as the stress path moves to the failure line. The effective stress then rises during the subsequent pore pressure dissipation, whilst the voids ratio reduces. During the subsequent cycles of sliding, and consolidation, the stress path follows a zig-zag pattern in stress:volume space with successive generation and dissipation of excess pore pressure. As the voids ratio approaches the critical state value for the stress imposed by the pipe, the level of excess pore pressure generation diminishes, and the asymptotic condition in which the drained and undrained sliding resistances are equal is approached. This causes the stress path in p:q space to become vertical.

Figure 6 also shows the stress path during the slow monotonic drained sliding case, which reaches the same ultimate state.

Strength changes beneath pipe invert

The cycles of shearing and consolidation cause a reduction in voids ratio and an increase in shear strength over a zone that extends well beyond the pipe invert. Figure 7 shows the increases in soil strength down a profile directly below the pipe invert. The soil strength profile is initially proportional to depth, with a value of s_u ~ 0.2 kPa at the pipe invert level. After consolidation under the vertical pipe load, this strength rises to ~0.5 kPa, but the cycles

of sliding and consolidation create a far greater rise in shear strength to an ultimate value of ~1.2 kPa. This variation in undrained strength is consistent with the rise in sliding resistance. The zone of significant strength gain extends ~0.5D beneath the pipe invert, which is consistent with experimental observations from model tests of axial pipe-soil interaction (Smith & White 2014).

CONCLUSIONS

It has been hypothesized that the axial sliding resistance between a pipe and the seabed on soft normally consolidated clay will rise from the initial undrained value to the drained limit, with a consequential benefit of reduced cyclic axial movement, or 'walking'. This effect has previously been analysed for the case of continuous sliding with concurrent consolidation. In this paper we provide the first theoretical quantification of this effect for episodic sliding, which comprises undrained movements interspersed with full consolidation.

It is shown that for Modified Cam clay, using properties representative of kaolin, the resistance rises exponentially with cycles and reaches the drained limit within approximately 20 episodes of movement and consolidation. The rise in resistance is accompanied by a corresponding increase in the strength of the soil surrounding the pipe.

The process of episodic shearing and intervening full consolidation means that the rate of gain in resistance is not dependent on the coefficient of consolidation of the soil, but varies with cycle number at a rate that depends on the ratio κ/λ.

ACKNOWLEDGEMENTS

The work described in this paper forms the part of activities at the Centre for Offshore Foundation Systems (COFS) at the University of Western Australia, currently supported as a node of the Australian Research Council Centre of Excellence for Geotechnical Science and Engineering. The second author is supported by Shell Australia, via the Shell EMI Chair of Offshore Engineering.

REFERENCES

Carr, M., Sinclair, F. & Bruton, D. 2006. Pipeline walking – understanding the field layout challenges, and analytical solutions developed for the SAFEBUCK JIP. Proc. Offshore Technology Conference, Houston. Paper OTC17945.

Chatterjee S., Yan, Y., Randolph M.F. & White D.J. 2012. Elastoplastic consolidation beneath shallowly embedded offshore pipelines. Géotechnique Letters, 2(2):73-79

Randolph, M.F., White, D.J. & Yan, Y. 2012. Modelling the axial soil resistance on deepwater pipelines. Géotechnique, 62(9):837-846

Roscoe, K.H. & Burland, J.B. 1968. On the generalised stress-strain behaviour of 'wet clay'. Engineering Plasticity, Cambridge University Press, 535-609.

Smith, V.B. & White D.J. 2014. Volumetric hardening in pipe-soil interaction. Proc. Offshore Technology Conference, Asia. Kuala Lumpur. Paper OTC24856MS

Tornes, K., Jury, J. and Ose, B. 2000. Axial creeping of high temperature flowlines caused by soil racheting. Proc. ASME Conf. on Offshore Mechanics and Arctic Engineering, OMAE-PIPE5055

White D.J. & Randolph M.F. 2007. Seabed characterisation and models for pipeline-soil interaction. Int. Journal of Offshore & Polar Engineering. 17(3):193-204

White D.J., & Cathie D.N. 2011. Geotechnics for subsea pipelines. Proc. 2nd Int. Symp. on Frontiers in Offshore Geotechnics. Perth. 87-123

White D.J., Bolton M.D., Ganesan S.A., Bruton D., Ballard J-C., Langford T. 2011. SAFEBUCK JIP: Observations from model testing of axial pipe-soil interaction on soft natural clays. Proc. Offshore Technology Conference, Houston. Paper OTC21249.

Wroth, C.P. 1984. The interpretation of in-situ tests. 24th. Rankine Lecture, Géotechnique, 34(4):449-489.

Yan, Y. 2014. Novel methods for characterising pipe-soil interaction forces in situ in deep water. PhD thesis, The University of Western Australia.

TABLES LIST

Table 1 Input parameters of numerical study

Soil property Parameters	Values
Slope of critical state line (CSL) in p'-q space, M (friction angle in triaxial compression, φ'_{tc}	0.92 (23.5°)
Void ratio at p' = 1 kPa on (CSL), e_{cs}	2.14
Slope of the virgin compression line in e-ln(p') space, λ	0.205
Slope of the swelling and recompression line in e-ln(p') space, κ	0.044
Elastic shear modulus, G	$50p_0'$
Saturated bulk unit weight, γ_{sat}: kN/m^3	15.0
Unit weight of water, γ_w: kN/m^3	10
Permeability of soil, k: m/s	1.0×10^{-9}
Consolidation coefficient at the pipe invert, c_{v0}: m^2/s	9.25×10^{-10}
Pipe diameter, D: m	0.5

Table 2 Values of T_{50} and constant m for Equation 1

Pipe Sweep No.	1	2	3	4	5	6	7	8 and beyond
m	1.20	1.15	1.10	0.95	0.94	0.90	0.90	0.90
T_{50}	0.0065	0.0060	0.0050	0.0044	0.0043	0.0042	0.0042	0.0041

FIGURE LIST

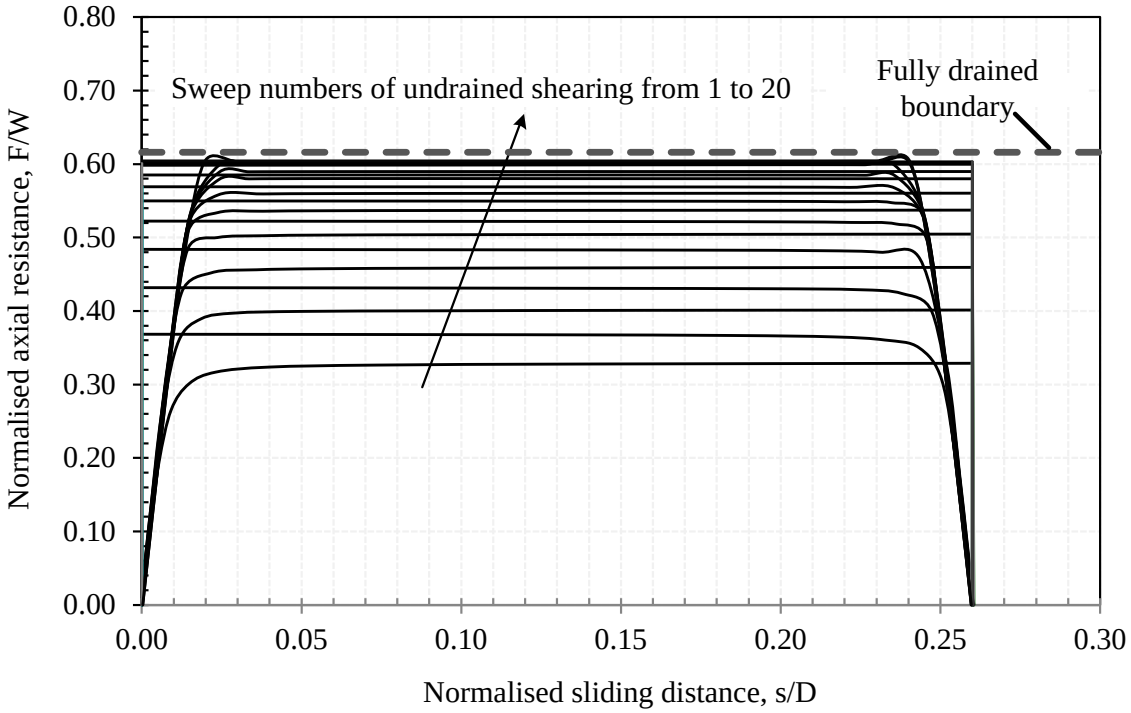

Figure 1 Axial sliding resistance-displacement responses for general pipe walking

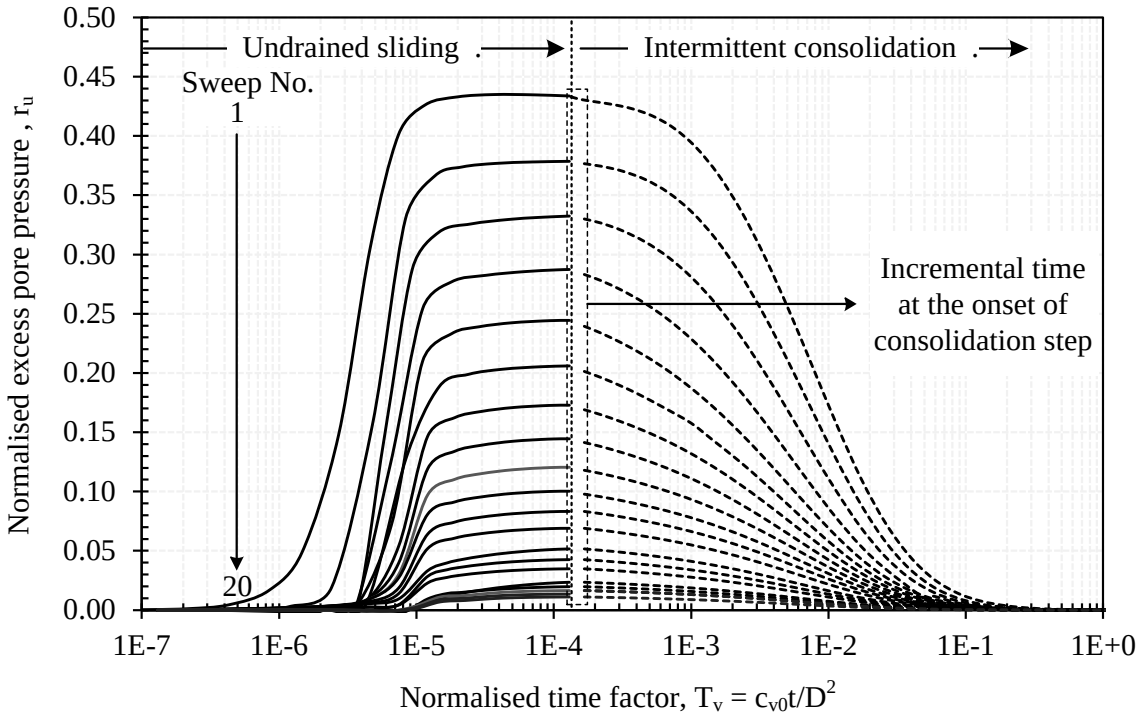

Figure 2 Excess pore pressure responses during general pipe walking

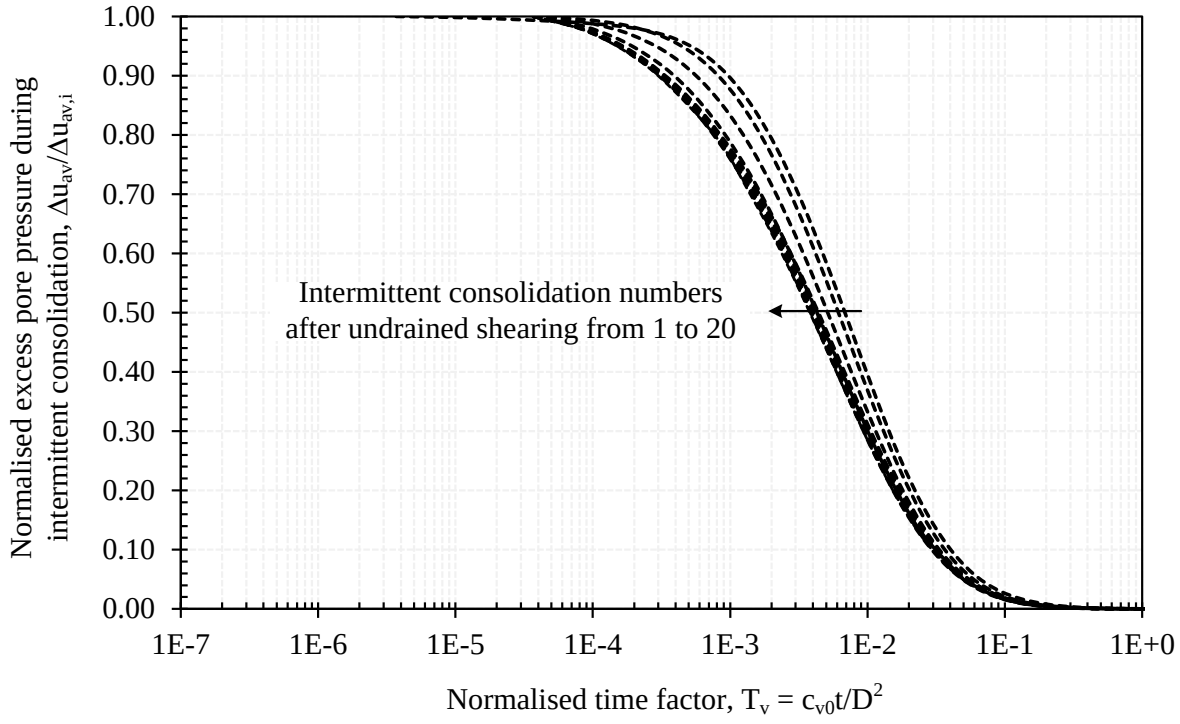

Figure 3 Normalised excess pore pressure responses after each undrained sweeps

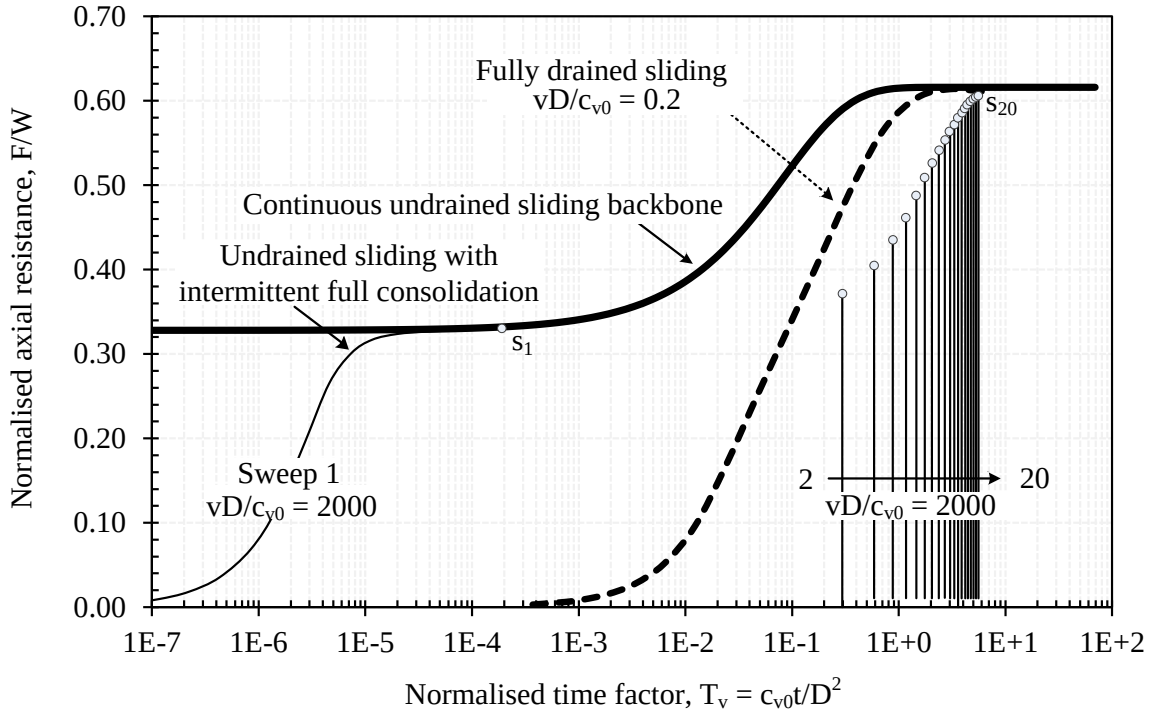

Figure 4 Consolidation curves for general pipe walking

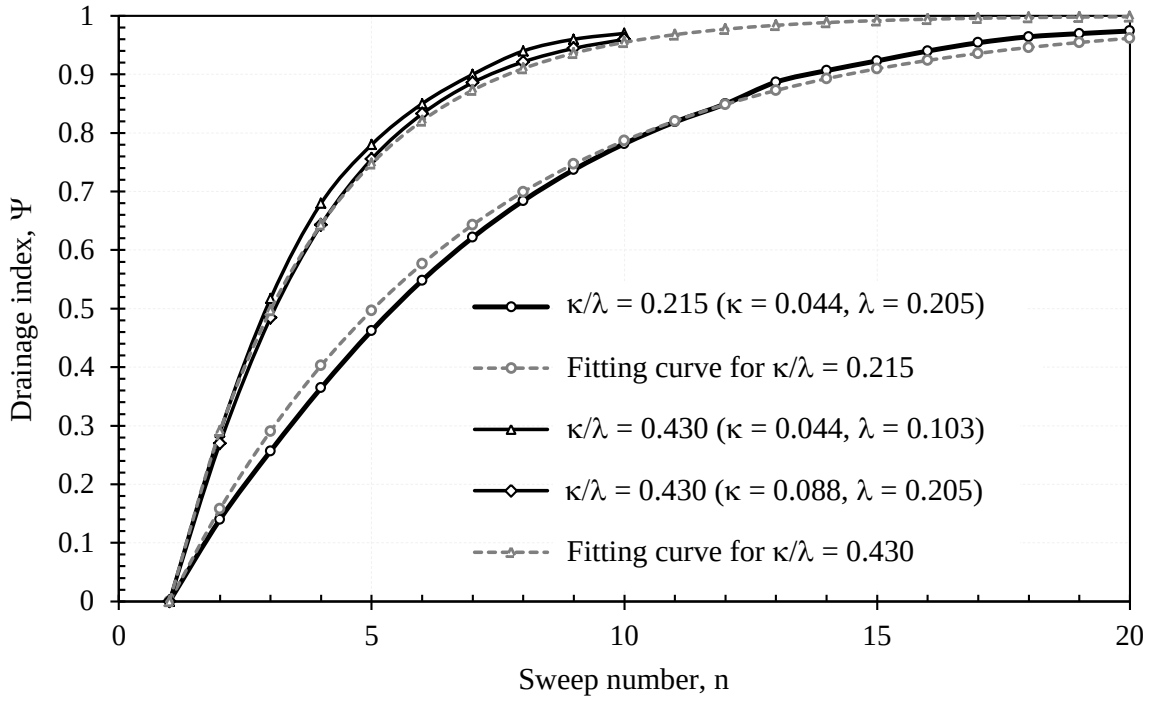

Figure 5 Gain in axial resistance with sweep number

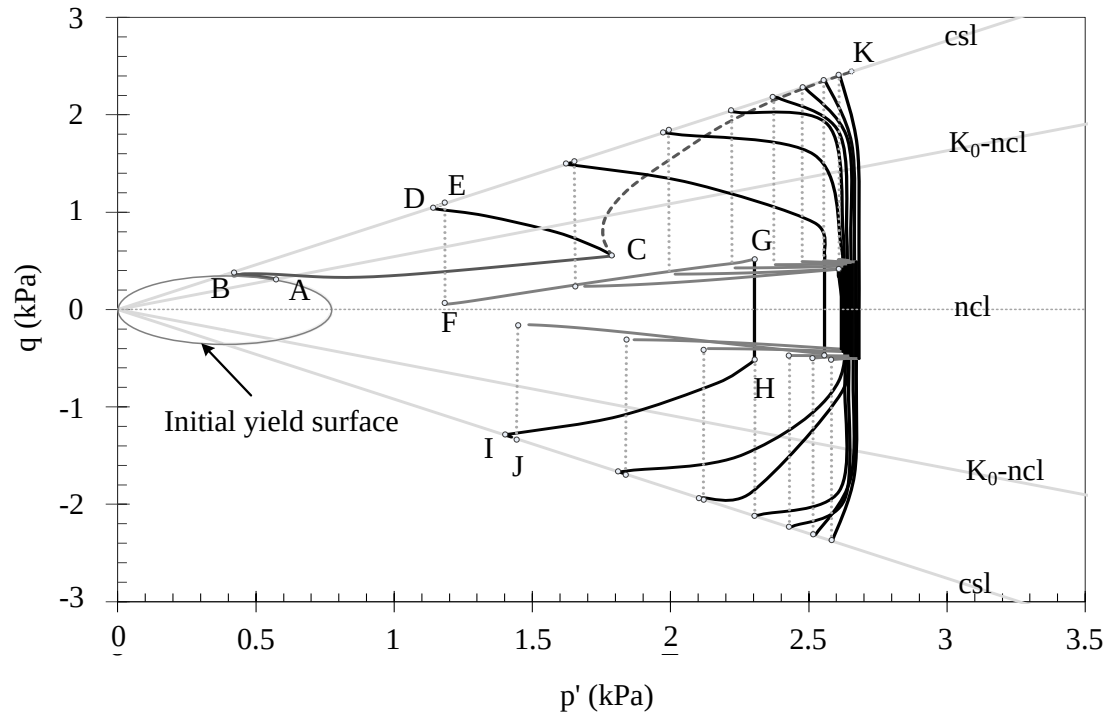

(a) Stress path

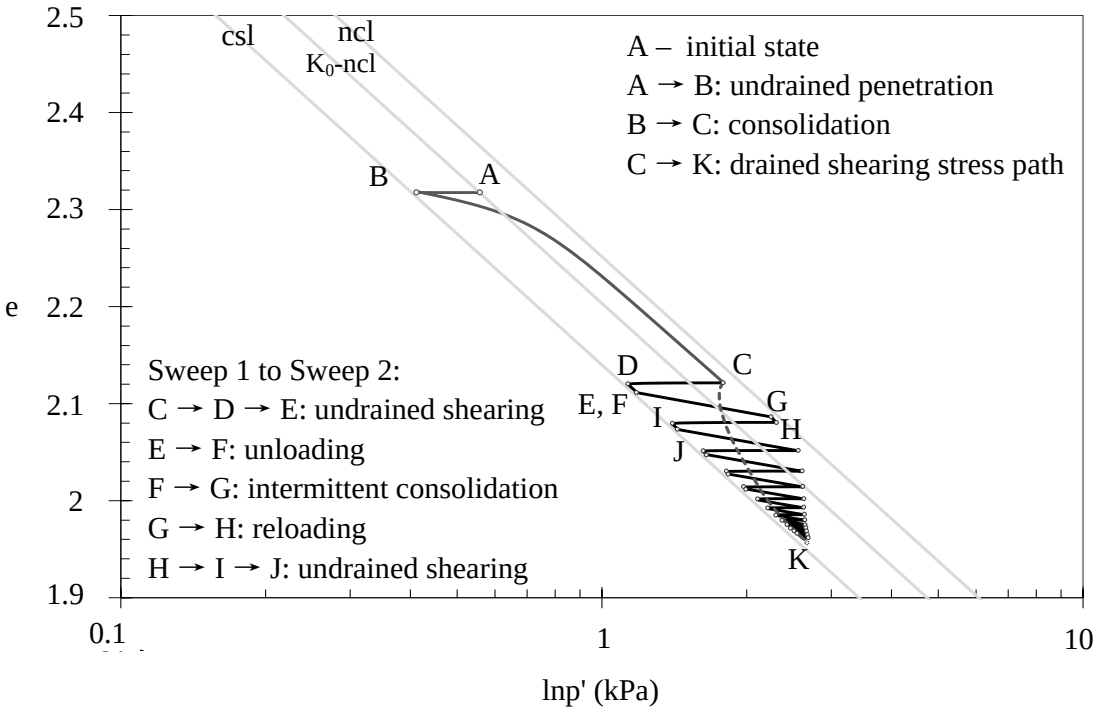

(b) Stress:volume path

Figure 6 Response of soil element beneath pipe invert

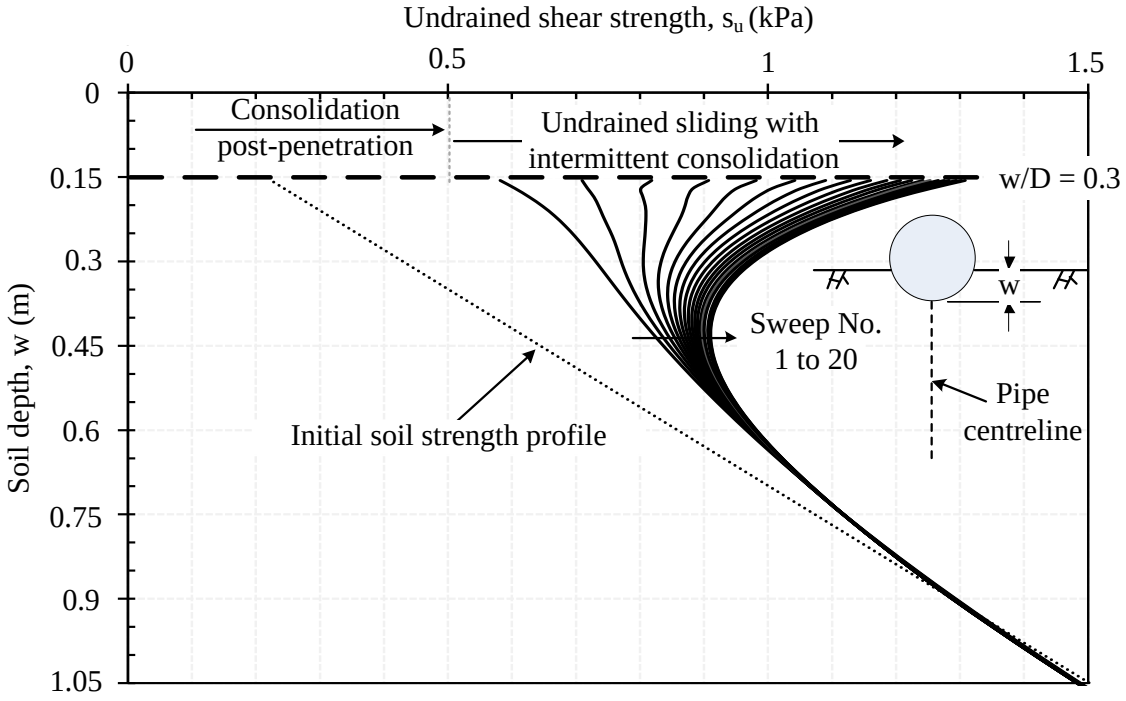

Figure 7 Profiles of normalised shear strength during and after general pipe walking